3D Object Detection with Normal-map on Point Clouds

Jishu Miao, Tsubasa Hirakawa, Takayoshi Yamashita and Hironobu Fujiyoshi
Chubu University, 1200 Matsumoto-cho, Kasugai, Aichi, Japan

Keywords: Object Detection, Deep Learning, Point Cloud Processing, Autonomous Vehicles.

Abstract: In this paper, we propose a novel point clouds based 3D object detection method for achieving higher-accuracy of autonomous driving. Different types of objects on the road has a different shape. A LiDAR sensor can provide a point cloud including more than ten thousand points reflected from object surfaces in one frame. Recent studies show that hand-crafted features directly extracted from point clouds can achieve nice detection accuracy. The proposed method employs YOLOv4 as feature extractor and gives Normal-map as additional input. Our Normal-map is a three channels bird's eye view image, retaining detailed object surface normals. It makes the input information have more enhanced spatial shape information and can be associated with other hand-crafted features easily. In an experiment on the KITTI 3D object detection dataset, it performs better than conventional methods. Our method can achieve higher-precision 3D object detection and is less affected by distance. It has excellent yaw angle predictability for the object, especially for cylindrical objects like pedestrians, even if it omits the intensity information.

1 INTRODUCTION

With the continuous development of autonomous driving technology, it will be possible to achieve higher levels of autonomous driving in the near future. All autonomous driving functions cannot be separated from the rapid development of computer vision and deep neural networks. The sensors currently equipped on autonomous vehicles are cameras, LiDARs, and radars. The information about the surrounding environment can be continuously captured and transmitted to the computer through these sensors. An autonomous vehicle can sense its surroundings and make correct operations.

LiDAR sensors emit pulsed light waves into the surrounding environment and receive the reflected points from object surfaces, which we call point clouds. Thus more than ten thousand points of information, including 3D coordinates and reflection intensities, can be obtained. Unlike RGB images, the significant advantages of point clouds are that they have obvious 3D spatial structure features and include reflection features about the surface of the object.

Autonomous vehicles need to have high-accuracy detection based on the sensors' information in a very short time. Object detection and classification based on deep learning are two crucial tasks that affect autonomous driving safety. The current mainstream object-detection method involves predicting the 2D bounding box's position, size, and class from images using region proposal networks (RPN) (Ren et al., 2015). This excellent object detection method can provide high-accuracy detection results while maintaining processing speed.

Point cloud is enormous and discontinuous, and there are currently various processing methods for extracting the hidden information in point cloud. The current method is to input processed information into a convolutional neural network then detect an object by using an RPN to identify object location and classification labels for the surrounding environment.

For further improvement of object detection accuracy, we propose a method based on *Normal-map*. This method includes the following characteristics. A normal is an object perpendicular to the given surface. Based on the spatial position information hidden in a point cloud, a normal can be estimated then used as the processed information to predict a 3D bounding box and classification labels through the convolutional neural network (CNN). There are significant shape differences between car bodies and cyclists. Moreover, roads and buildings have regular shapes, thus almost the same surface normals. Our method extracts powerful spatial information from point clouds while reducing the dimensions of the cloud.

Miao, J., Hirakawa, T., Yamashita, T. and Fujiyoshi, H.
3D Object Detection with Normal-map on Point Clouds.
DOI: 10.5220/0010304305690576
In *Proceedings of the 16th International Joint Conference on Computer Vision, Imaging and Computer Graphics Theory and Applications (VISIGRAPP 2021) - Volume 5: VISAPP*, pages 569-576
ISBN: 978-989-758-488-6

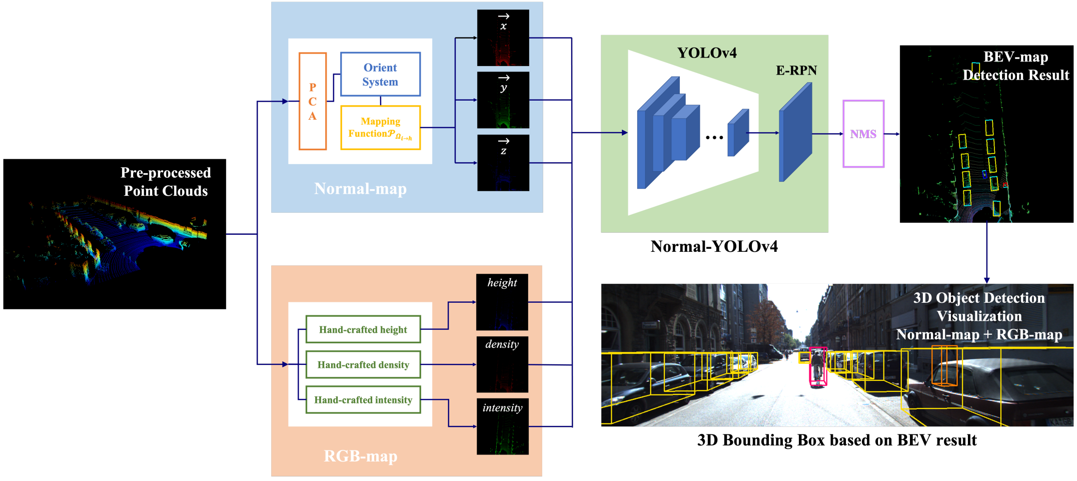

Figure 1: **Overview of the proposed method.** Our method detects 3D objects by using YOLOv4 + Euler-Region Proposal Network (E-RPN). The input feature is a combination of Normal-map and RGB-map (see Section 3.1) to improve the precision of 3D object detection, especially for cylindrical objects.

The contributions of this paper are as follows:

- We introduce a well-designed normal estimation pipeline, extract estimated surface normals to Normal-map, integrate it into the whole system as additional input.
- With the addition of Normal-map, input information is enhanced. We show that Normal-map can achieve better object detection accuracy and maintain stable performance on objects in different levels of difficulty.
- The proposed method has the potential to compensate for the effects of a lack of reflection intensity. Under a no-reflection intensity condition, it can still achieve high-precision object detection.

2 RELATED WORK

2.1 2D Object Detection

The CNN can achieve high-precision 2D object detection based on a single image. There are two types of object detection approaches. The first type is a two-stage detector: Regions with CNN feature (R-CNN) (Girshick et al., 2014), Fast R-CNN (Girshick, 2015), and the newest one called Faster R-CNN (Ren et al., 2015) with a 12-fold improvement in detection speed. Two-stage detectors have a low error detection rate and low missing rate.

Another type is a one-stage detector: it inferences the classification scores, and bounding boxes of objects, and the final detection result can be obtained directly through only one phase. Therefore, compared with two-stage detectors, they have a faster detection speed, the most typical one-stage detectors are SSD (Liu et al., 2016), and YOLO (Redmon et al., 2016)(Redmon and Farhadi, 2017)(Redmon and Farhadi, 2018)(Bochkovskiy et al., 2020). These methods have laid the foundation to make it possible for real-time object detection.

2.2 3D Object Detection

Due to the need for autonomous driving, it is important to perform real-time 3D object detection. Based on the important feature of a point cloud containing 3D spatial structure information, there is an increasing number of 3D object detection methods depending on the type of deep learning network's input, i.e. point cloud (Shi et al., 2019), voxel (Simon et al., 2019), or image (Beltrán et al., 2018).

MV3D (Chen et al., 2017) involves two types of point cloud processes. One is to construct a bird's eye view (BEV) image. Each pixel is the highest point in the grid. Each layer of a grid is used as a channel, then intensity and density values are added. The other type is to construct a front view (FV) image. The point cloud is projected into the cylindrical coordinate system, then rasterized to form 2D grids in the cylindrical coordinate, then construct height, intensity and density channels are constructed. The accuracy of this method is high, but due to the large amount of calculation, the processing speed is only 2.8 fps.

Complex-YOLO (Simony et al., 2018) is a method focused on the efficiency, that has the same point cloud process as the first one of MV3D (Chen et al., 2017). The point clouds are only converted into three

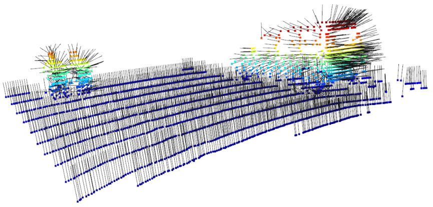

Figure 2: Surface normals estimated from point clouds.

channels BEV images (called as RGB-map), which are put into YOLOv2, just like with RGB images. It detects objects only in the BEV image then increases the dimension and angle in the final regression variable, which solves the problem of 3D object detection and ensures real-time processing speed at the same time.

2.3 Surface Normal Estimation

The surface normal is an important property of the geometric surface and often used in many areas. If a geometric surface is given, it is usually easy to estimate the normal of a point on this surface as a vector perpendicular to the surface located on that point. A point cloud is composed of thousands of points reflected back from the surface of an object, therefore it is a precise record on the shape of the object.

There is a well-known method for estimating surface normals on point clouds. It involves estimating surface normals directly from the point cloud using approximation. Liu *et al.* proposed a normal estimation method (Ran et al., 2013) for point cloud. It speeds up the searching process by using the *kd*-tree tree data structure (Merry et al., 2013) to find the neighbor field. The normal estimation by *kd*-tree is robust. Wang *et al.* (Wang and Siddiqi, 2016) proved that adding first and second-order features such as surface normal and curvature is helpful in improving the object detection performance.

Open3D (Zhou et al., 2018) is an open-source library that supports the rapid development of software that handles 3D data. We used the Open3D library to estimate correct and regular surface normals directly from a point cloud.

3 PROPOSED METHOD

This study focuses on further improvement of the accuracy of 3D object detection on point clouds. Our 3D object detection method is based on surface normals as they are important spatial information. This method not only simply extracts point clouds but also extracts object surface shape information to Normal-map by normal estimation. Through increasing the amount of input information and using the YOLOv4 network, the accuracy of 3D object detection is further improved.

3.1 Point Cloud Processing

Different from object detection on RGB images, point clouds are sparse, and a huge amount of computation is necessary if the point clouds are directly input to a convolutional neural network. Therefore, we generate hand-crafted BEV-map in two ways for each frame of point clouds. Based on the surface normal estimation of point clouds, and inspired by MV3D (Chen et al., 2017), we created a 3 channel BEV RGB-map by extracting values from point cloud.

Since both YOLOv3 (Redmon and Farhadi, 2018) and YOLOv4 (Bochkovskiy et al., 2020) exhibit excellent detection performance at an input size of 608, the BEV grid map size is defined as (608×608) and set the LiDAR position as the origin of the Cartesian coordinate system as follows:

$$P_{\Omega} = [x, y, z]^T \tag{1}$$

The select points within an area of 50 m long and 50 m wide (i.e, $x \in [0, 50]$ and $y \in [-25, 25]$). Considering that the LiDAR sensor is located at 1.73m, we set the range of z axis to $[-2.73, 1.27]$, so that it can cover all objects within a height range of about 4m from the ground. Based on the above settings, each pixel of the BEV image can carry information within the actual $50 meter/608 = 8cm$ range.

3.1.1 Normal Estimation

We estimate the surface normals to hold as much of the object shape features as possible for the point in this area. We use an approximate method to estimate normals directly from the point cloud. The normal of a point will be inferred from its surrounding points.

The surface normal is brought by principal component analysis (PCA) of the covariance matrix C created from the nearest neighbors of the target point p_i.

$$C = \frac{1}{k} \sum_{i=1}^{k} (p_i - \overline{p}) \cdot (p_i - \overline{p})^T \tag{2}$$

$$C \cdot \vec{v}_j = \lambda_i \cdot \vec{v}_j, \quad j \in \{0, 1, 2\} \tag{3}$$

Here, k is the number of neighbor points considered near p_i, $\overline{p}$ is the nearest 3D centroid, λ_j is the eigenvalue of the covariance matrix in j, and $\vec{v}_j$ is the eigenvector of j. If $0 \leq \lambda_0 \leq \lambda_1 \leq \lambda_2$, the eigenvector v_0 of the smallest eigenvalue λ_0 is the approximate value of normal vector $\vec{n}$.

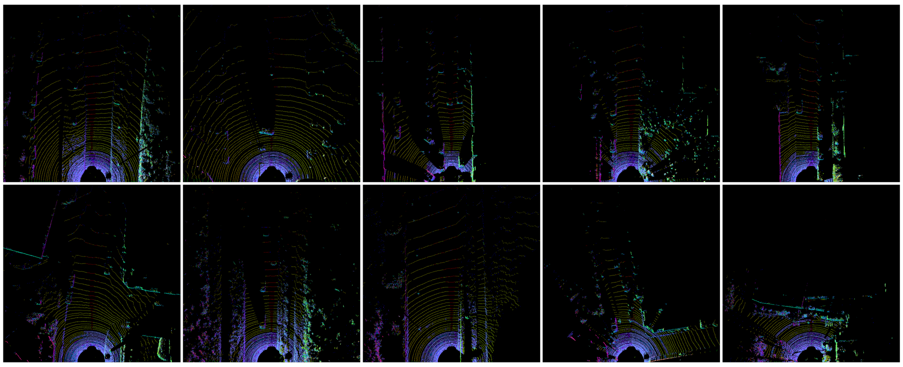

Figure 3: **The Visualization of Normal-map.** A 2D BEV feature map based pseudo-image contains the 1st-order features (surface normal) of objects.

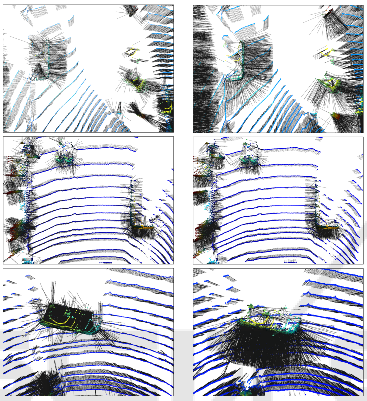

(a) Raw Normal (b) After Orient

Figure 4: Align results of Orient System in BEV.

Considering the efficiency of directly finding neighbor points, we use the *kd*-tree algorithm, a data structure known for high computation efficiency.

In this study, we set the searching range of the normal estimation to 30 cm and search for a maximum of 50 points near the target point. Due to this setting, under a resolution of (608×608), the normal vector (1st-order feature) actually overcomes the limitations of the 0th-order features which are limited by the representation range $(8cm/pixel)$. It is possible to present surface normals beyond the pixel range.

3.1.2 Camera Relative Coordinate System

Without knowing the object geometric structure, a normal vector generally has two directions and are both correct. This kind of randomness would confuse the convolutional neural network to a certain extent. For consistent orientation of a point cloud, it is necessary to satisfy:

$$\vec{n}_i \cdot (\mathrm{v}_p - \mathrm{p}_i) > 0 \tag{4}$$

In order to solve this problem, we designed a normal orient system for ensuring the consistency of the final normal vector:

- **Orient System:** It follows the actual state of point clouds, which are emitting and reflecting back to the LiDAR. Since LiDAR is set at an altitude of 1.73m above the ground, we orient all normal vectors toward $(0,0,0)$ in LiDAR coordinate.

Some examples of orient system's output is shown in Fig. 4. Comparing with the raw normals in Fig. 4(a), there are more consistent normals after orienting by the camera relative coordinate system in Fig. 4(b).

3.1.3 Generate Normal-map

The estimated normal is a set of 3D unit vector containing $(\vec{x}, \vec{y}, \vec{z})$. In this study, we converted normal vectors into a 2D BEV pseudo-image, which we call *Normal-map*. The mapping function $\mathcal{S}_j = f_{\mathcal{PS}}(\mathcal{P}_{\Omega i}, g)$ is used for mapping each point into a specific grid cell $\mathcal{S}_j$ of Normal-map, which describes all the points in $\mathcal{P}_{\Omega i \to j}$:

$$\mathcal{P}_{\Omega i \to j} = \{\mathcal{P}_{\Omega i} = [x,y,z]^T | \mathcal{S}_j = f_{\mathcal{PS}}(\mathcal{P}_{\Omega i}, g)\} \tag{5}$$

Through this, we only keep the point with the biggest z value, the $\mathcal{P}_{\Omega j \to h}$ describes every highest point in each grid cell at range$[0,4]$ meter. We then extract each point's normal vector from $\mathcal{P}_{\Omega j \to h}$ to $normal_{\vec{x}}$, $normal_{\vec{y}}$, $normal_{\vec{z}}$ by axis.

$$\begin{aligned} normal_{\vec{x}}(\mathcal{S}_j) &= \vec{x}(\mathcal{P}_{\Omega j \to h}), \\ normal_{\vec{y}}(\mathcal{S}_j) &= \vec{y}(\mathcal{P}_{\Omega j \to h}), \\ normal_{\vec{z}}(\mathcal{S}_j) &= \vec{z}(\mathcal{P}_{\Omega j \to h}). \end{aligned} \tag{6}$$

In normal-map, each channel indicates the normal vector of the highest point in the grid cell, corresponding to that channel. Besides, the 0th-order feature maps: density, intensity, and height map of RGB-map are also extracted.

$$\begin{aligned} z_r(\mathcal{S}_j) &= \min(1.0, \log(N+1)/64), N = |\mathcal{P}_{\Omega i \to j}| \\ z_g(\mathcal{S}_j) &= \max(\mathcal{P}_{\Omega i \to j} \cdot [0,0,1]^T) \\ z_b(\mathcal{S}_j) &= \max(I(\mathcal{P}_{\Omega i \to j})) \end{aligned} \tag{7}$$

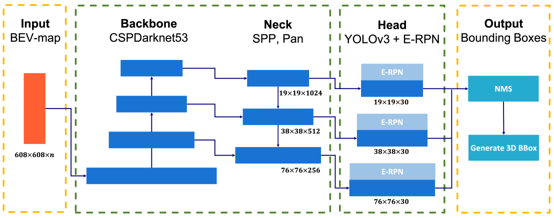

Figure 5: Normal-YOLOv4 network architecture.

Thus, there are 4 hand-crafted pseudo-images: in Normal-map, $normal_{\vec{x}}$, $normal_{\vec{y}}$, $normal_{\vec{z}}$ encodes normal vectors $(\vec{x}, \vec{y}, \vec{z})$; In RGB-map, z_r is the normalized density of all points in $\mathcal{S}_j$, z_g is the maximum height, and z_b is the maximum intensity.

3.2 Network Input

We will not lose any information for separating 3D normal vectors into three channels. An RGB image is composed of three RGB channels, as does Normal-map. Normal-map can represent spatial geometric information when three channels are combined, just like in RGB images. The benefit of this is that the Normal can combine with other BEV feature maps and apply 2D convolution. We combine Normal-map with RGB-map at the object detect network's first layer as input images. Thus, the network input will be a n-dimensional array depending on the combination of BEV-maps.

3.3 Network Architecture

Our Normal-YOLOv4 object detection network employs the YOLOv4 (Bochkovskiy et al., 2020) to extractor features from the input BEV-map, extended it by an Euler-Region Proposal Network (E-RPN) to regress angle and detect multi-class 3D objects.

As shown in Fig. 5, the input is a n-dimensional (608×608) 2d-pseudo image, the n is depend on the channels of the BEV-map combination. Then neck outputs the multi-scale feature maps to the head in size: $(76 \times 76 \times 256)$, $(38 \times 38 \times 512)$, and $(19 \times 19 \times 1024)$. The head is based on YOLOv3, and added E-RPN as the extension, giving network the ability to accurately predict object angles. The head finally predicts a 10 dimensions output for each box: object position (t_x, t_y), object dimensions (t_w, t_l), object angles (t_{im}, t_{ie}), as well as probability p_0, class scores p_1, p_2, p_3.

In each grid cell, we predict three boxes resulting in 30 features each. The object angle is calculated as $\arctan(t_{im}, t_{re})$. Due to the height is not as important as other information in the autonomous driving, we use a predefined height h to build 3D bounding box for conserving computational resources. Thus, Normal-map would not affect the prediction of height directly.

3.4 Loss Function

In Normal-YOLOv4, YOLOv3 is used as the head as same as the YOLOv4. In this study, the loss function is Mean-square Error (MSE), which is based on YOLOv3, and the angle loss calculation is added for angle regression. Since the network is a combination of YOLOv4 and E-RPN, the entire loss function is presented as follows.

$$\mathcal{L} = \mathcal{L}_{\text{YOLO}} + \mathcal{L}_{\text{E-RPN}} \tag{8}$$

$$\mathcal{L}_{\text{E-RPN}} = \lambda_{coord} \sum_{i=0}^{S^2} \sum_{j=0}^{B} \mathbb{1}_i j^{obj} [(t_{im} - \hat{t}_{im})^2 + (t_{re} - \hat{t}_{re})^2] \tag{9}$$

Therefore, The yaw can be calculated as $\arctan(Im, Re)$ and adjust all the parameters continuously through back-propagation.

4 EXPERIMENTS

In this section, we evaluate the performance of the proposed method on the KITTI benchmark for bird's eye view. Our ablation studies compare the object detection precision of Normal-map with RGB-map in different Intersection over Union (IoU) threshold and distance. We also evaluate the accuracy of the model in predicting the yaw angle by adding an included angle function.

4.1 KITTI Dataset

There are three types of KITTI object detection evaluation (Geiger et al., 2012): 2D, 3D and BEV. For the proposed method, we chose dataset both point clouds and left color images data. It contains 7481 frames training data including annotated ground truth and 7518 frames testing data without public ground truth. All the data were randomly disrupted and the previous and next frames were not from the same scene. We use only point cloud for object detection and the color images for visualizing the results.

4.2 Training Details

The training data is split in a ratio of 4 : 1. There are 6000 samples in training data were only used for the network training, and the remaining 1481 samples with their ground truth labels were for validation

Table 1: Evaluation Results for Bird's eye view Performance on the KITTI Benchmark (Test data).

Method		Car AP (%)			Pedestrian AP (%)			Cyclist AP (%)			mAP (%)
	FPS	Easy	Mod.	Hard	Easy	Mod.	Hard	Easy	Mod.	Hard	
BirdNet	9.1	**84.17**	59.83	57.35	**28.20**	**23.06**	**21.65**	**58.64**	**41.56**	**36.94**	**45.93**
Complexer-YOLO	16.7	77.24	68.96	64.95	21.42	18.26	17.06	32.00	25.40	22.88	38.68
Ours	5.5	72.84	**71.52**	**67.50**	26.71	21.19	20.17	42.50	36.06	31.18	43.30

Table 2: Performance of models with different sets of inputs.

Input	Hand-crafted features				Classes AP			mAP
	Normal-map	RGB-map			*Car*	*Pedestrian*	*Cyclist*	(%)
	$(\vec{x},\vec{y},\vec{z})$	density	height	intensity	(%)	(%)	(%)	IoU 50
RGB	-	√	√	√	96.26	76.83	90.10	87.73
Normal	√	-	-	-	97.78	71.57	89.28	86.21
Normal+RG	√	√	√	-	97.38	78.58	91.18	89.05
Normal+RGB	√	√	√	√	96.90	85.57	94.50	**92.325(↑4.60)**

and the evaluation of ablation study. We regarded both "Cars" and "Vans" as *Cars* and both "Pedestrian" and "Person (sitting)" as *Pedestrians*. So that the network would learn how to classify three classes: *Cars*, *Pedestrian* and *Cyclists*. Model was trained from scratch using the Adam optimizer. The cosine decay is applied to the learning rate.

Based on the Bag of freebies (BoF) of YOLOv4's backbone, data augmentation (i.e. including horizontal flip, scaling, random crop, mosaic and random padding) is applied for the input 2D BEV pesudo-images during network training. It enriches the number of datasets but would not change the connection between pixels and values on BEV-map. In ablation study, all experimental sets were trained in 200 epochs, making the results reliable enough.

4.3 Network Performance

The prediction results of the official test set are evaluated by the KITTI Vision Benchmark Suite for BEV benchmark. We focus on the BEV performance of the proposed method.

As shown in Table 1. The proposed method (Ours) achieves 72.84% for class *Car* in Easy difficulty, and guarantee 67.50% in Hard difficulty at the same time. Facing the objects of the same category but different difficulty, the addition of surface normal makes the detecting more robust, especially for the objects with regular surface shapes like cars.

Based on the statistics provided by the KITTI leaderboard, we compare the proposed method to two state-of-the-art methods. Compared to BirdNet (Beltrán et al., 2018), a BEV-based object detection network, proposed method demonstrates better detection performance on *Car* at higher levels of difficulty. The proposed method achieves better mean average precision (mAP) in BEV detection than Complexer-YOLO (Simon et al., 2019), which is known as employ YOLOv3 network. Although the input of proposed method is 2D pseudo-image, not the 3D voxelized semantic point clouds, the accuracy of objects with highly non-planar surface (i.e., pedestrian and cyclist) is still higher in any level of difficulty.

4.4 Ablation Studies

To confirm the effectiveness of the proposed method, we combined Normal-map with other hand-crafted features in three different sets, as shown in Table. 2. We used the point cloud processing described in Section 3.1, calculated all the features we need.

mAP for Object Detection. All three classes used the same Intersection over Union (IoU) threshold. As shown in Eq. 10, the IoU is given by the overlapping area between the predicted bounding box B_{pred} and the ground truth bounding box B_{gt} divided by the area of union.

$$IoU \quad = \quad \frac{area(B_{pred} \cap B_{gt})}{area(B_{pred} \cup B_{gt})}. \qquad (10)$$

Table 2 shows that Normal+RGB set achieves the highest mAP of 91.94 in all sets of this ablation study. Besides, proposed method achieves better precision balance than RGB-map-only set, which proves the effectiveness of Normal-map

According to the Table 3. Normal-based methods have higher mAP than RGB-map-only set with different IoU threshold. In addition, when the reflection intensity is removed, the set with Normal-map still achieves a higher mAP. This means that Normal-map has the potential to be used in environments where reflection strength is unreliable.

Evaluation over Distance. The point cloud at near-by is relatively dense but sparse of the further object. In this experiment, the objects are divided into five sets according to their distance of LiDAR position,

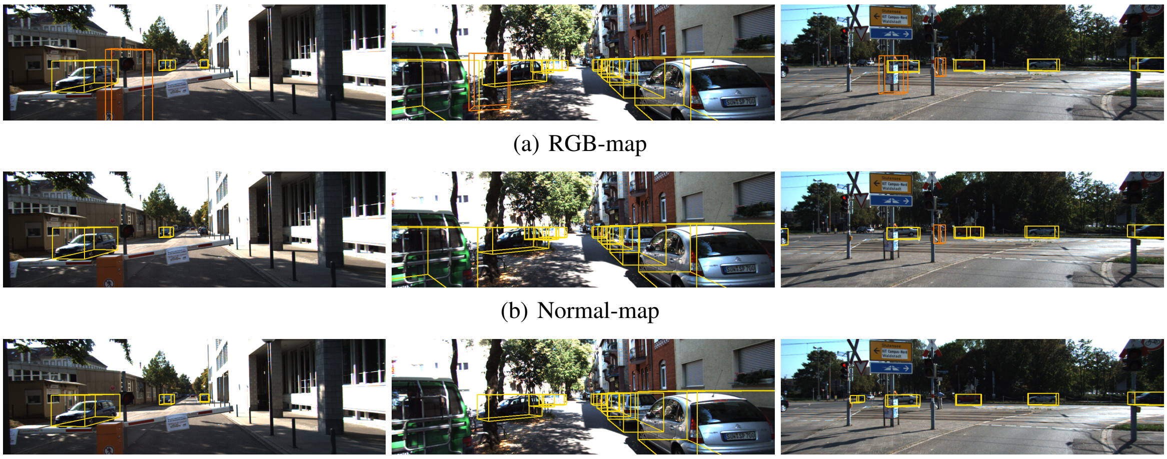

(a) RGB-map

(b) Normal-map

(c) Normal-map + RGB-map

Figure 6: **3D object detection visualization in camera view**. Three different feature combination sets were compared. With addition of Normal-map, false detection of cylindrical object, which is similar to pedestrian, significantly decreased, especially for three left images.

Table 3: mAP with different IoU threshold.

	IoU Threshold				
Feature	0.5	0.6	0.7	0.8	0.9
RGB	87.7	77.5	55.6	24.1	0.8
Norm.	86.2	82.2	66.3	38.5	4.7
Norm.+RG	89.1	83.2	61.8	31.9	2.4
Norm.+RGB	92.3	89.0	79.3	53.8	17.3

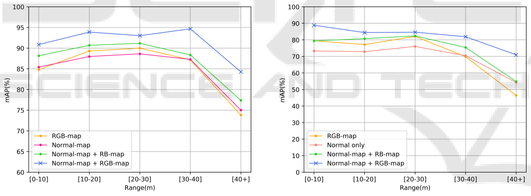

(a) mean AP

(b) Pedestrian AP

Figure 7: **Average precision of object detection over distance.** Pedestrian AP of RGB-map set fell down rapidly with the distance increasing, while the Normal-based sets were less affected by it.

and calculated the average precision of objects in each set.

It is shown in Fig. 7(a) that all experimental sets have similar trends. The mAP is higher in mid-range, because the mid-range of global coordinate is the centre area in BEV image. We can find that all sets with the addition of Normal-map have a significant improvement comparing with RGB-map only. With the increasing distance, point clouds become sparse leading mAP falls down in all sets. The PCA based surface normal estimation is known to be sensitive to the surface curvature. But we can see the results of [40+] in Fig. 7(a), all Normal-based sets still have better accuracy than RGB-map only.

Yaw Angle Error Evaluation. As the surface normal is a spatial shape information of an object, we think Normal-map could improve the object yaw angle accuracy. In this study, object yaw angle is brought by $\arctan(Im, Re)$.

Considering that in the Cartesian coordinate system, both π and $-\pi$ are actually pointed in the same direction, the yaw angle error cannot be calculated from predicted yaw and gt directly. Thus we assume that the predicted yaw angle is a (Im_p, Re_p) vector and the ground truth is (Im_{gt}, Re_{gt}). The accuracy of the yaw angle can be evaluated by comparing the size of included angle θ between $\vec{a}_p$ and $\vec{b}_{gt}$. The evaluation scores of each class are calculated as Eq. 12 shows:

$$\vec{a}_p \boldsymbol{.} \vec{b}_{gt} = |\vec{a}_p||\vec{b}_{gt}|cos\theta \tag{11}$$

$$score_{class}(\theta_k) = (\frac{1}{n}\sum_{k=1}^{n} \arccos\theta_k)^{-1} \tag{12}$$

As shown in Fig. 8, Normal-based method has smaller included angles which means Normal-map is conducive to accuracy improvement of object yaw angle. In addition, Normal-map is been used as only input can still further improve the yaw angle accuracy for the object with more flat and large planar surface.

Visualization Results. As can be seen from Figs. 6, the traffic sign and traffic light were incorrectly detected as cyclists or pedestrians in the results of RGB-map. This result shows cylindrical objects and those are similar in height to humans would confuse the model and cause it to predict incorrectly. Normal-map seldom results in such mistakes because humans definitely have a different shape than traffic lights or signs. Objects with a highly non-planar surface like

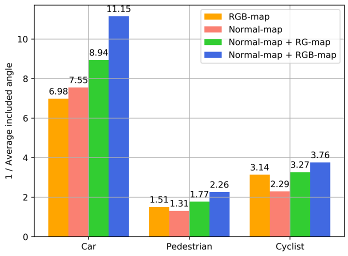

Figure 8: Accuracy of yaw angle prediction of 3 classes.

pedestrians have significantly precision improvement on object detection with the help of Normal-map.

5 CONCLUSION

In this work we propose a 3D object detection method that combines Normal-map (the surface normal estimated from point cloud) with other hand-crafted images. The proposed method makes the input information have more enhanced spatial shape information. The object detection results show competitive performance on KITTI benchmarks. This method has better accuracy in object detection than conventional methods, and is less affected by sparse point clouds. In addition, it brings better yaw angle prediction. It also has excellent anti-interference ability for object surfaces with unreliable reflection intensity data. Our method has the potential to be used for the virtual-world dataset, enables further research in autonomous driving. In the future, we would like to use a modern normal estimation technique in our pipeline for the accuracy of Normal-map go further. We also plan to improve it to detect more classes of objects and faster.

REFERENCES

Beltrán, J., Guindel, C., Moreno, F. M., Cruzado, D., García, F., and Escalera, A. D. L. (2018). Birdnet: A 3d object detection framework from lidar information. In *2018 21st International Conference on Intelligent Transportation Systems (ITSC)*, pages 3517–3523.

Bochkovskiy, A., Wang, C.-Y., and Liao, H.-Y. M. (2020). Yolov4: Optimal speed and accuracy of object detection. *arXiv preprint arXiv:2004.10934*.

Chen, X., Ma, H., Wan, J., Li, B., and Xia, T. (2017). Multi-view 3d object detection network for autonomous driving. In *The IEEE Conference on Computer Vision and Pattern Recognition (CVPR)*.

Geiger, A., Lenz, P., and Urtasun, R. (2012). Are we ready for autonomous driving? the kitti vision benchmark suite. In *Conference on Computer Vision and Pattern Recognition (CVPR)*.

Girshick, R. (2015). Fast r-cnn. In *Proceedings of the IEEE international conference on computer vision*, pages 1440–1448.

Girshick, R., Donahue, J., Darrell, T., and Malik, J. (2014). Rich feature hierarchies for accurate object detection and semantic segmentation. In *The IEEE Conference on Computer Vision and Pattern Recognition (CVPR)*.

Liu, W., Anguelov, D., Erhan, D., Szegedy, C., Reed, S., Fu, C.-Y., and Berg, A. C. (2016). Ssd: Single shot multibox detector. In *European conference on computer vision*, pages 21–37. Springer.

Merry, B., Gain, J., and Marais, P. (2013). Accelerating kd-tree searches for all k-nearest neighbours. Technical report, University of Cape Town.

Ran, L., Ximin, Z., Yiyuan, Z., Wanggen, W., and Libing, L. (2013). Normal estimation algorithm for point cloud using kd-tree. *IET International Conference on Smart and Sustainable City 2013 (ICSSC 2013)*.

Redmon, J., Divvala, S., Girshick, R., and Farhadi, A. (2016). You only look once: Unified, real-time object detection. *2016 IEEE Conference on Computer Vision and Pattern Recognition (CVPR)*.

Redmon, J. and Farhadi, A. (2017). Yolo9000: Better, faster, stronger. In *The IEEE Conference on Computer Vision and Pattern Recognition (CVPR)*.

Redmon, J. and Farhadi, A. (2018). Yolov3: An incremental improvement. *arXiv preprint arXiv:1804.02767*.

Ren, S., He, K., Girshick, R., and Sun, J. (2015). Faster r-cnn: Towards real-time object detection with region proposal networks. In *Advances in neural information processing systems*, pages 91–99.

Shi, S., Wang, X., and Li, H. (2019). Pointrcnn: 3d object proposal generation and detection from point cloud. In *Proceedings of the IEEE Conference on Computer Vision and Pattern Recognition*, pages 770–779.

Simon, M., Amende, K., Kraus, A., Honer, J., Samann, T., Kaulbersch, H., Milz, S., and Michael Gross, H. (2019). Complexer-yolo: Real-time 3d object detection and tracking on semantic point clouds. In *Proceedings of the IEEE Conference on Computer Vision and Pattern Recognition Workshops*, pages 0–0.

Simony, M., Milzy, S., Amendey, K., and Gross, H.-M. (2018). Complex-yolo: An euler-region-proposal for real-time 3d object detection on point clouds. In *Proceedings of the European Conference on Computer Vision (ECCV)*, pages 0–0.

Wang, C. and Siddiqi, K. (2016). Differential geometry boosts convolutional neural networks for object detection. In *The IEEE Conference on Computer Vision and Pattern Recognition (CVPR) Workshops*.

Zhou, Q.-Y., Park, J., and Koltun, V. (2018). Open3d: A modern library for 3d data processing. *arXiv preprint arXiv:1801.09847*.